

Lead-acid cells with polyaniline-coated negative plates

S.K. MARTHA¹, B. HARIPRAKASH¹, S.A. GAFFOOR² and A.K. SHUKLA^{1,3,*}

¹*Solid State and Structural Chemistry Unit, Indian Institute of Science, Bangalore 560 012, India*

²*NED Energy Ltd., 6-3-1109/1 Navbharat Chambers, Raj Bhavan Road, Hyderabad 500 082, India*

³*Central Electrochemical Research Institute, Karaikudi 630 006, India*

(*author for correspondence, tel.: +91-80-22932795, fax: +91-80-23601310, e-mail: shukla@sscu.iisc.ernet.in)

Received 13 July 2005; Accepted in revised form 27 January 2006

Key words: lead-acid battery, polyaniline, hybrid electric vehicles

Abstract

Positive- and negative-limited lead-acid cells with conventional and polyaniline (PANI)-coated negative plates were assembled and tested at varying discharge rates. The cells with PANI-coated negative plates exhibit lower impedance in relation to conventional cells and sustain higher discharge-rates with lesser loss in capacity during prolonged charge–discharge cycling as compared to conventional cells. It is suggested that PANI-coated negative plates are beneficial in designing lead-acid batteries operating at partial-state-of-charge.

1. Introduction

In certain applications, such as hybrid electric-vehicles, the lead-acid battery is required to operate almost all the time at partial-state-of-charge and to supply and receive charge at unprecedented rates [1–3]. Since high-rate discharge cannot proceed into the interior of the negative plates, the utilization of the active material remains low [4–6]. Besides, the relative density of sulfuric acid after discharge is still at a high level, which decreases the dissolution of PbSO₄ [7–9]. As a consequence, the lower concentration of Pb²⁺-ions impedes the subsequent electrochemical reaction, and during the early stage of battery charging, causes the negative plate potential to become more negative so much so that H₂ can start to evolve. Furthermore, the electrons flowing from the grid towards the surface of the plate, reduce some hydrogen ions to H₂ gas prior to reacting with the PbSO₄ layer. Accordingly, the complete conversion of PbSO₄ at the plate surfaces cannot be achieved even with an over-charge due to the combined effects of the early evolution of H₂ and the O₂-recombination reaction. This leads to rapid accumulation of PbSO₄ on the negative plate leading to early failure of the lead-acid battery [9–28].

In this study we have addressed the aforesaid problems by electrochemically introducing PANI into the negative active mass of both the positive- and negative-limited lead-acid cells. It is inferred that a minimal degradation in the structure and conductivity of the negative active material occurs in such cells, enabling them to sustain high discharge-rates with prolonged cycling capability.

2. Experimental

2.1. Preparation of PANI-coated negative plates

Cured negative plates were placed in a bath containing 1 v/o aqueous solution of aniline in 0.15 M oxalic acid with each plate held between two symmetrically placed dimensionally stable platinum-coated-titanium electrodes. A thin layer of PANI was subsequently electrodeposited onto the plates by applying a potential of 1.4 V across the plates and the counter electrodes [29]. The plates were finally washed copiously with de-ionized water and dried in a hot air oven at about 65 °C.

2.2. Assembly of positive-limited lead-acid cells

2V/7Ah conventional positive-limited lead-acid cells were assembled by stacking two cured positive plates and three cured conventional negative plates (hereafter referred as type 1) while 2V/7Ah positive-limited lead-acid cells with PANI-coated negative plates were assembled by stacking two cured positive plates and three cured PANI-coated negative plates (hereafter referred as type 2). Positive and negative plates in the cells were separated by placing 2 mm thick AGM separator obtained from Nippon Sheet Glass Co., Japan. The plates were strapped with polythene bands and connected to their respective lugs. Prior to formation, the cells were filled with required amounts of 4.5 M aqueous sulfuric acid and kept for 2 h for electrolyte soaking in polypropylene containers.

2.3. Assembly of negative-limited lead-acid cells

2V/7Ah conventional negative-limited lead-acid cells were assembled by stacking three cured positive plates and two cured conventional negative plates (hereafter referred as type 3) while 2V/7Ah negative-limited lead-acid cells with PANI-coated negative plates were assembled by stacking three cured positive plates and two cured PANI-coated negative plates (hereafter referred as type 4). Positive and negative plates in the cells were separated by placing 2 mm thick AGM separator obtained from Nippon Sheet Glass Co., Japan. The plates were strapped with polythene bands and connected to their respective lugs. Prior to formation, the cells were filled with required amounts of 4.5 M aqueous sulfuric acid and kept for 2 h for electrolyte soaking in polypropylene containers.

2.4. Formation and testing of lead-acid cells

All the type 1, type 2, type 3, and type 4 lead-acid cells were formed over 3 cycles by charging them galvanostatically at C/10 rate followed by discharge at C/5 rate using an automated Keithley 228 A voltage/current source interfaced to a data-acquisition system. The cells were charged/discharged at varying rates at temperatures ranging between -20 and 50 °C in temperature-controlled chambers.

2.5. Self-discharge studies on lead-acid cells

To obtain self-discharge data on all the type 1, type 2, type 3, and type 4 lead-acid cells, the type 1 and type 2 cells were stored for 45 days and type 3 and type 4 cells were stored for 30 days at 25 °C, and their discharge-capacity values were obtained at C/5 rate using a Keithley 228 A voltage/current source interfaced to a data-acquisition system.

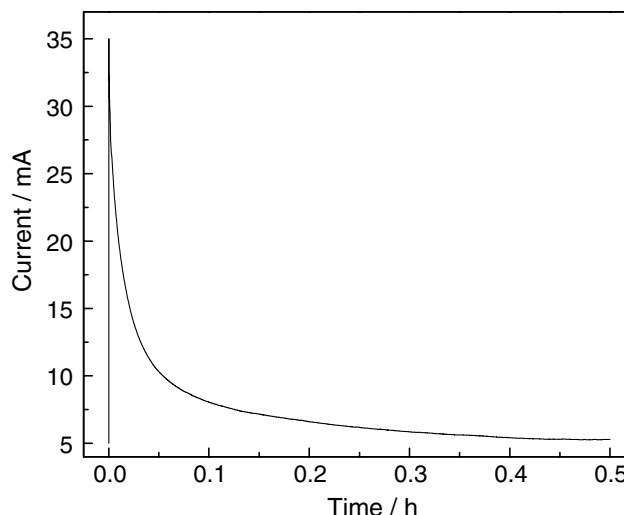


Fig. 1. Current vs. time response during PANI film formation at 1.4 V on a 43 cm^2 cured conventional negative plate in presence of oxalic acid by potential-step technique.

2.6. Cycle-life studies on lead-acid cells

Cycle-life data on all the type 1, type 2, type 3, and type 4 lead-acid cells were obtained for about 100 cycles at 25 °C, using a Keithley 228 A voltage/current source interfaced to a data-acquisition system. For this purpose the cells were discharged up to 1.75 V at C/5 rate.

2.7. Surface morphology of the negative plates

Powder X-ray diffraction (XRD) patterns of the conventional negative and PANI-coated negative plates both in fully-charged and discharged states were recorded on a Philips X-ray Diffractometer using $\text{CuK}\alpha$ -radiation ($\lambda = 1.5418 \text{ \AA}$) at a scan rate of 2° min^{-1} . Surface morphologies of the conventional negative and PANI-coated negative plates in their cured, fully-charged and fully-discharged states were examined

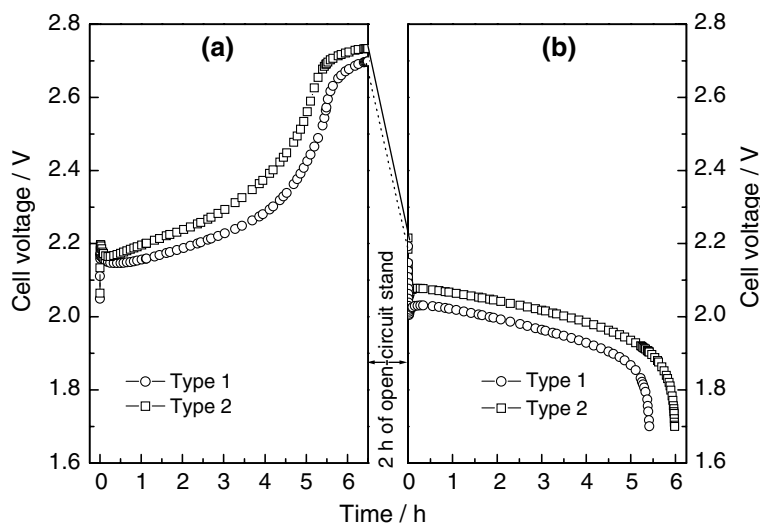


Fig. 2. Typical (a) charge and (b) discharge data obtained at 25 °C at C/5 rate for type 1 and type 2 lead-acid cells.

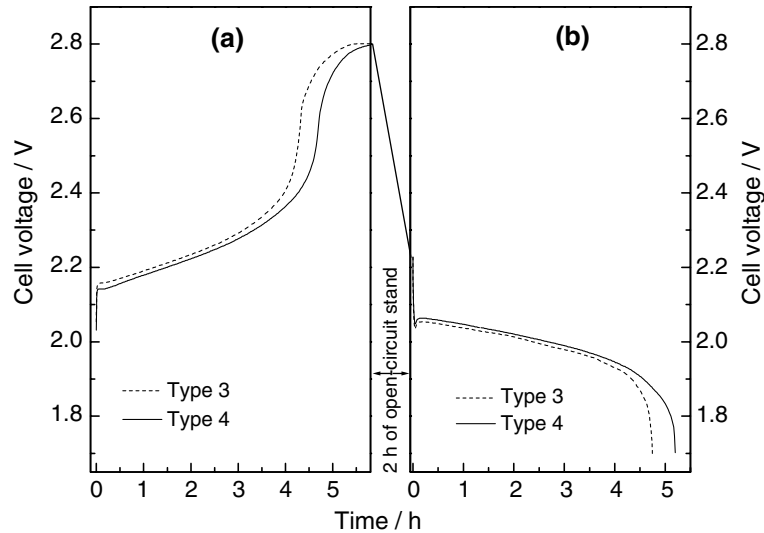


Fig. 3. Typical (a) charge and (b) discharge data obtained at 25 °C at C/5 rate for type 3 and type 4 lead-acid cells.

using a JEOL JSM-5600LV Scanning Electron Microscope. PANI film was characterized by recording its infra-red (IR) spectrum on a Perkin–Elmer Infra-Red Spectrophotometer.

2.8. Impedance studies on lead-acid cells

Impedance measurements at various SoC values on all the type 1, type 2, type 3, and type 4 lead-acid cells were carried out in the frequency range between 10 kHz and 5 mHz by employing an Autolab PGSTAT 30 instrument. The cells were discharged to various voltages and the SoC values were fixed by taking 1.75 V as SoC=0.

The impedance parameters of the cells were evaluated from the experimental impedance spectrum employing an equivalent-circuit non-linear least square (NLLS)-fitting procedure due to Boukamp [30]. The NLLS-fit technique was employed using an appropriate circuit description code (CDC): (RL) R (RQ) (RQ), where R, L, and Q stand for the circuit resistance, inductance and constant phase element, respectively. The elements within parentheses represent their parallel combination, while those without parentheses represent the series combination. The starting values were obtained from the Data Cruncher sub-program prior to using the values in the NLLS-fit program.

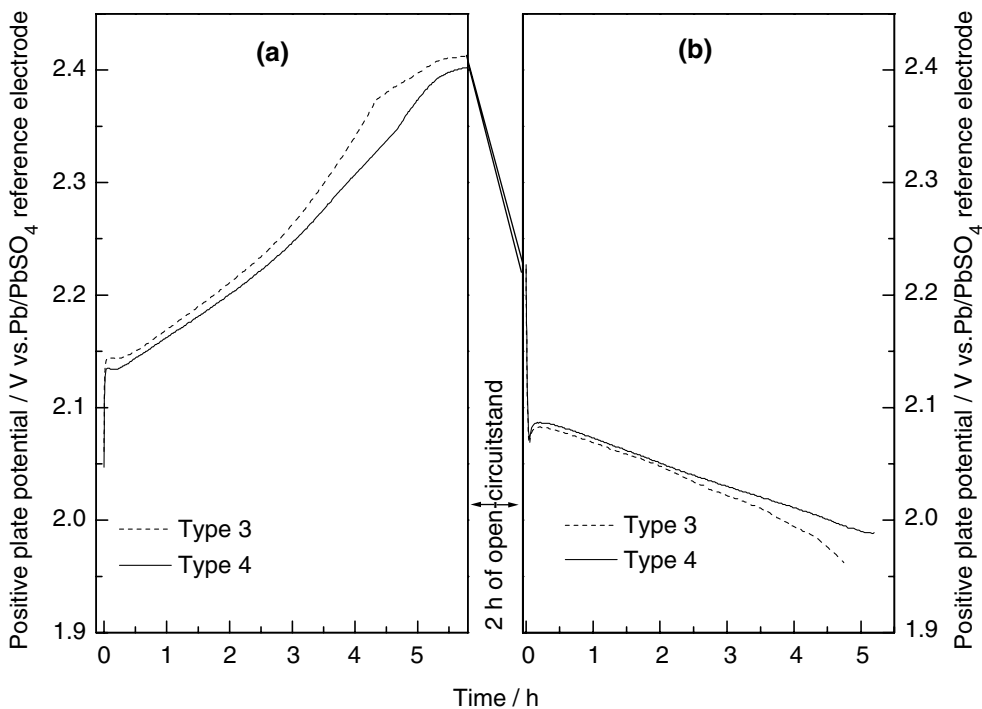


Fig. 4. Typical (a) charge and (b) discharge data obtained at 25 °C at C/5 rate for positive plates of type 3 and type 4 lead-acid cells.

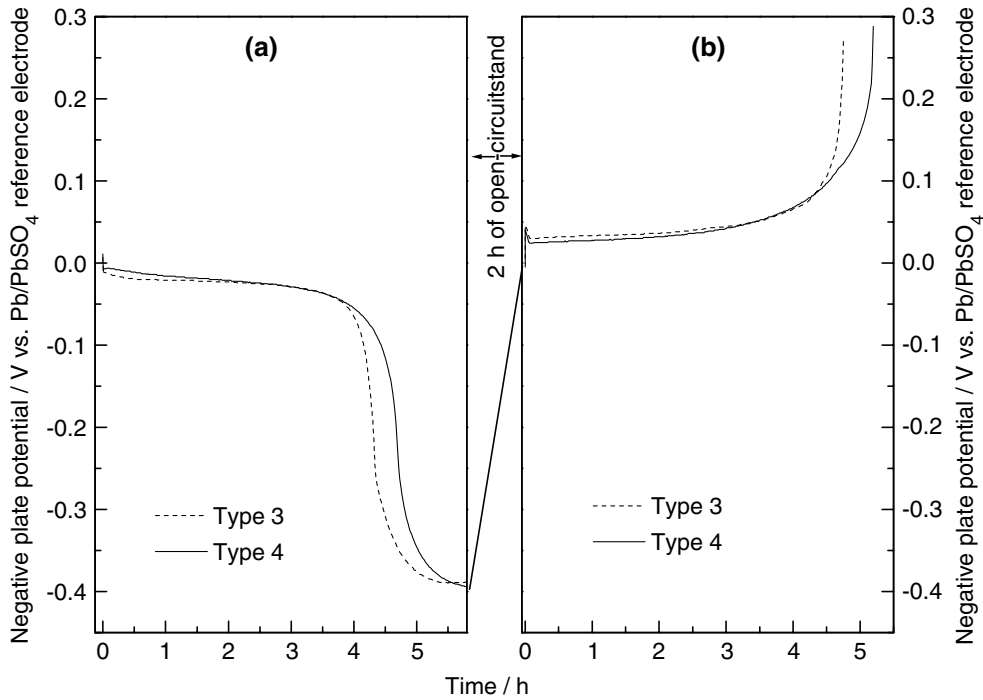


Fig. 5. Typical (a) charge and (b) discharge data obtained at 25 °C at C/5 rate for negative plates of type 3 and type 4 lead-acid cells.

3. Results and discussion

The growth pattern of the PANI film on a 43 cm² area cured conventional negative plate is depicted in Figure 1. It is noteworthy that the film growth in oxalic acid is quite different to that in sulfuric acid owing to the reducing nature of the former. All the type 1, type 2, type 3, and type 4 lead-acid cells were assembled and subjected to formation. The cells are found to form within three formation cycles and attain their rated

capacity. During the formation, the cells are charged at C/10 rate followed by their discharge at C/5 rate. Subsequent to formation, the typical charge/discharge data obtained at 25 °C at C/5 rate for type 1 and type 2 lead-acid cells are shown in Figure 2. It is found that the faradaic efficiency of type 2 cells (92%) is higher in relation to type 1 cells (85%). The type 2 cell also delivers higher discharge capacity than a type 1 cell.

The charge/discharge data for type 3 and type 4 lead-acid cells obtained at 25 °C at C/5 rate are shown in

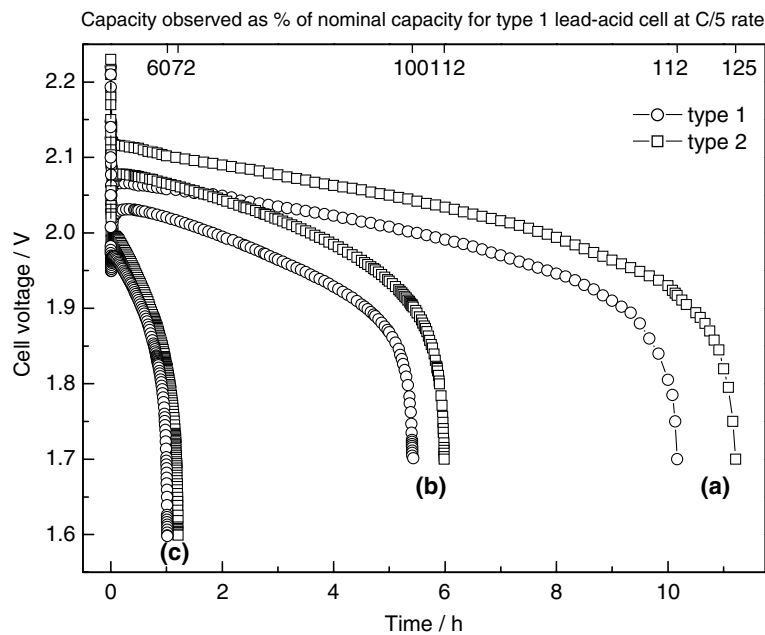


Fig. 6. Performance characteristics of type 1 and type 2 lead-acid cells at 25 °C at (a) C/10, (b) C/5, and (c) C-rates.

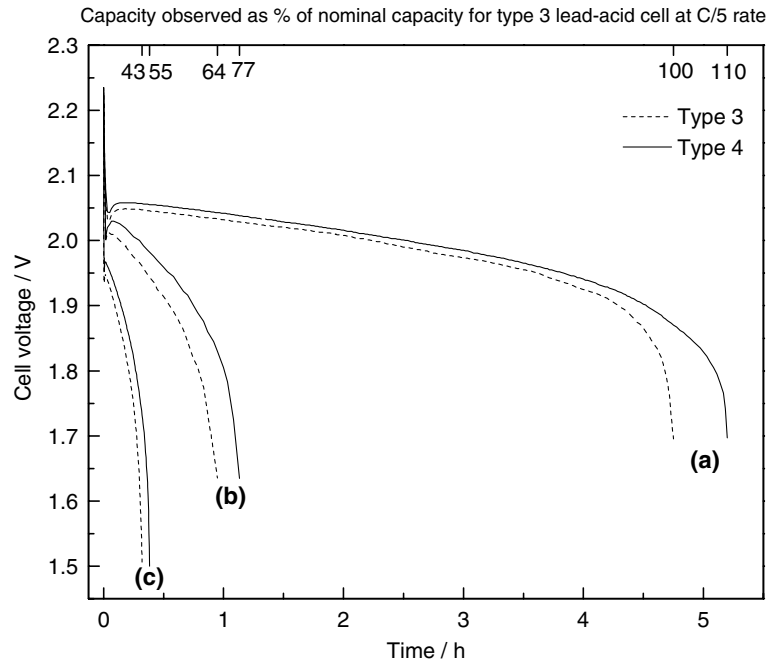


Fig. 7. Performance characteristics of type 3 and type 4 lead-acid cells at 25 °C at (a) C/5, (b) C, and (c) 3C-rates.

Figure 3. Here, also, the faradaic efficiency of type 4 cells is higher (92%) than type 3 cells (84%). The positive plate charge/discharge data for type 3 and type 4 lead-acid cells are shown in Figure 4. There is little difference in the positive plate charge data both for type 3 and type 4 lead-acid cells. The negative plate charge/discharge data for type 3 and type 4 lead-acid cells are shown in Figure 5. It is found that PANI-coated negative plates accept higher charge than the conventional negative plates. Accord-

ingly, type 4 lead-acid cells deliver higher negative-plate capacity than type 3 lead-acid cells.

Performance characteristics of type 1 and type 2 lead-acid cells at different rates ranging between C/10 and C are depicted in Figure 6 in relation to % of normal capacity for type 1 lead-acid cell obtained at C/5 rate. It is seen that, type 2 lead-acid cells deliver 72% capacity at C-rate as against 60% obtained with the type 1 cells. Similarly, performance characteristics of type 3 and type

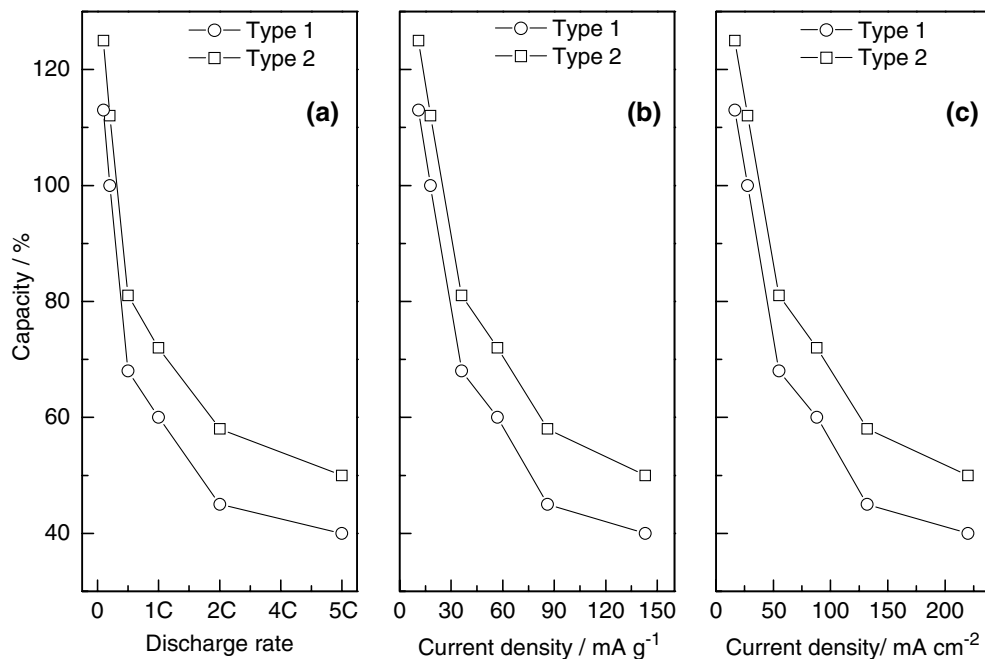


Fig. 8. Percentage capacities obtained at 25 °C for type 1 and type 2 lead-acid cells at different (a) discharge rates, (b) current densities in terms of weight, and (c) current densities in terms of area.

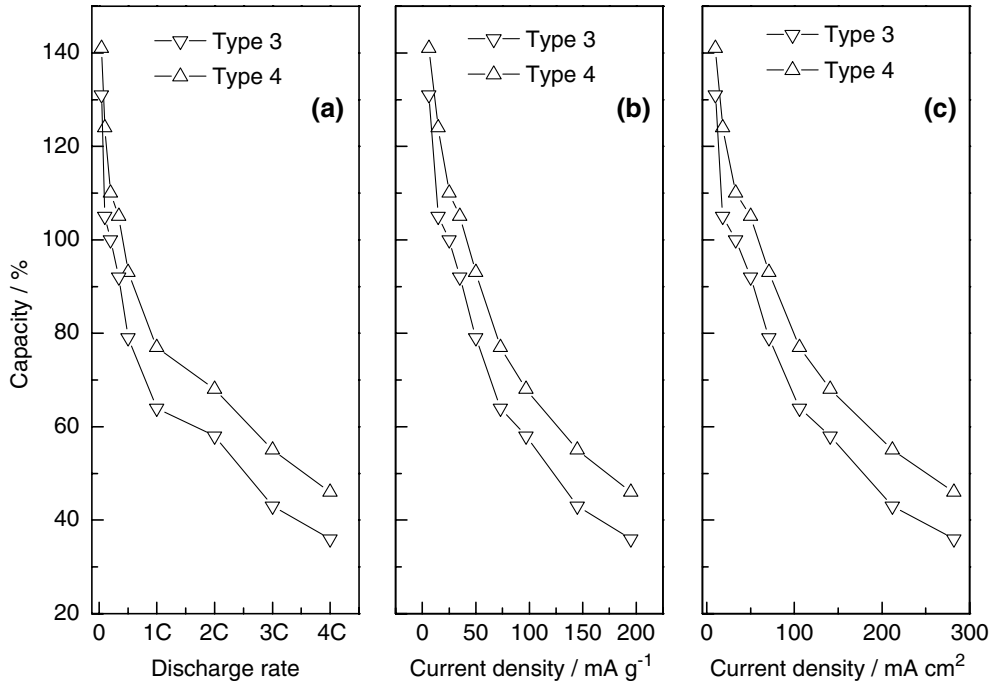


Fig. 9. Percentage capacities obtained at 25 °C for type 3 and type 4 lead-acid cells at different (a) discharge rates, (b) current densities in terms of weight, and (c) current densities in terms of area.

4 lead-acid cells at different rates ranging between C/5 and 3C are depicted in Figure 7 as % of nominal capacity for type 3 lead-acid cells at C/5 rate. Type 4 lead-acid cells deliver 77% capacity at C-rate as against 64% obtained with the type 3 lead-acid cells. The cells

with PANI-coated negative plates have lower internal resistance and provide a wider effective capacity window as shown in Figures 6 and 7.

Figure 8 shows the relative capacity data (in %) obtained at 25 °C for type 1 and type 2 lead-acid cells

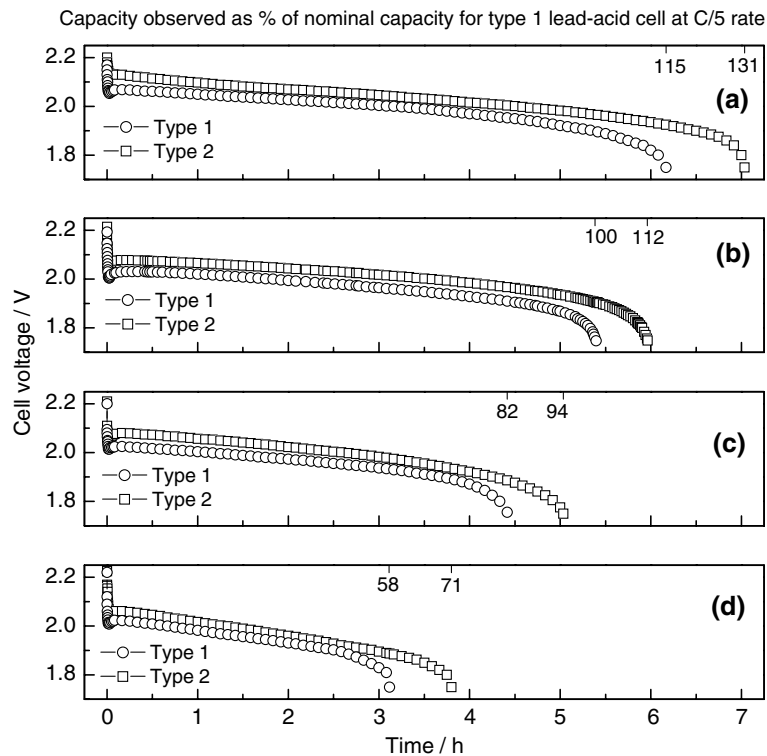


Fig. 10. Temperature-dependent discharge capacity data for type 1 and type 2 lead-acid cells at C/5 rate at (a) 50 °C, (b) 25 °C, (c) 0 °C, and (d) -20 °C.

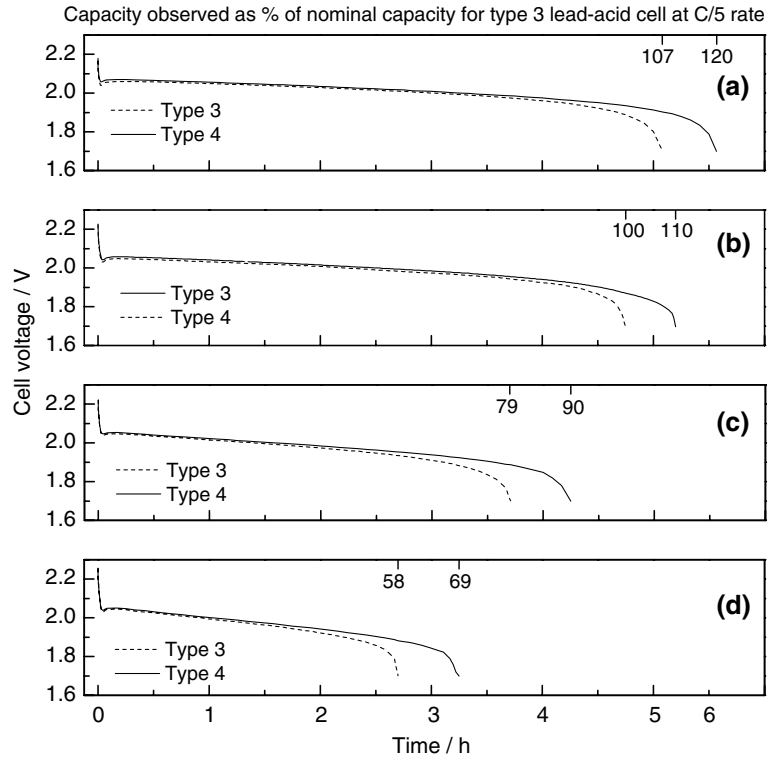


Fig. 11. Temperature-dependent discharge capacity data for type 3 and type 4 lead-acid cells at C/5 rate at (a) 50 °C, (b) 25 °C, (c) 0 °C, and (d) -20 °C.

at (a) different discharge rates, (b) varying current densities, in terms of weight, and (c) varying current densities, in terms of area. Similar data, for type 3 and type 4 lead-acid cells are shown in Figure 9. Taking the capacity of both type 1 and type 3 lead-acid cells at C/5 rate as 100%, a considerable increase

in the capacity of both type 2 and type 4 cells is observed at all discharge-rates. For example, an increase in discharge-capacity of almost 10–12% is seen at all discharge current densities for both type 2 and type 4 lead-acid cells in relation to type 1 and type 3 lead-acid cells.

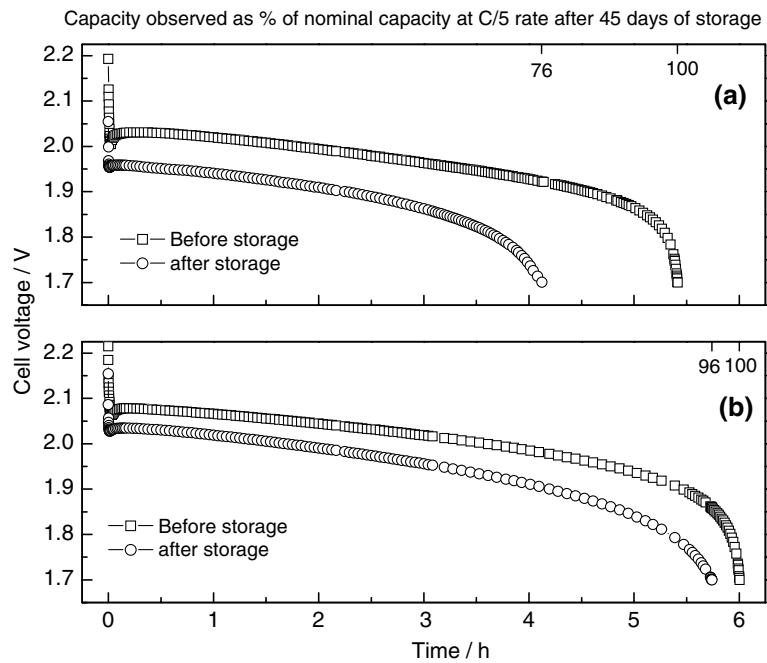


Fig. 12. Self-discharge data obtained at C/5 rate (□) before storage and (○) after 45 days of storage for (a) type 1 and (b) type 2 lead-acid cells at 25 °C.

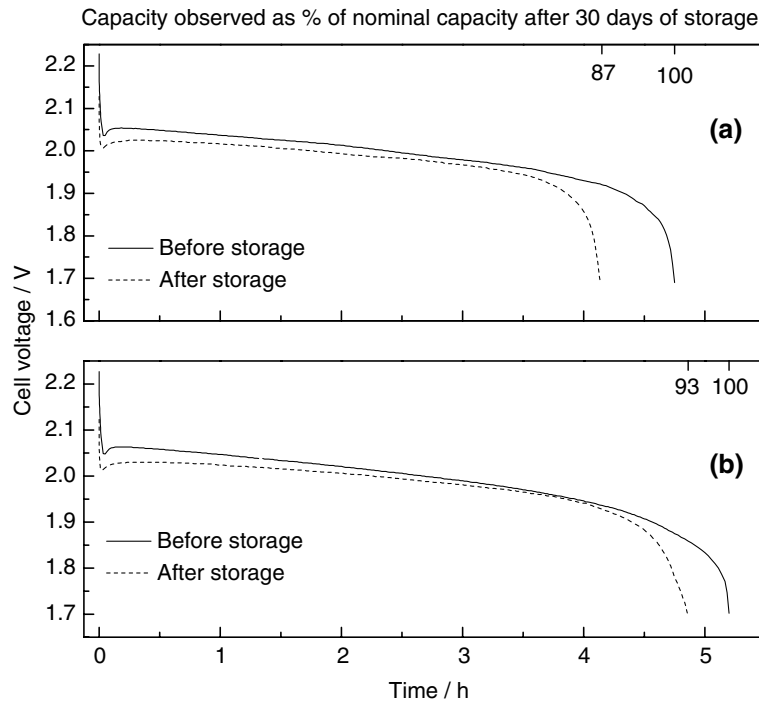


Fig. 13. Self-discharge data obtained at C/5 rate (—) before storage and (---) after 30 days of storage for (a) type 3 and (b) type 4 lead-acid cells at 25 °C.

Figures 10 and 11 show the discharge data for type 1, type 2, type 3 and type 4 lead-acid cells at C/5 rate at different temperatures between -20 and 50 °C. The data show that type 2 and type 4 lead-acid cells perform better than type 1 and type 3 lead-acid cells at all temperatures. The type 2 lead-acid cells deliver about 71% and 131% capacity at -20 and 50 °C, respectively, in relation to the respective values of 58% and 115% obtained for type 1 lead-acid cells. Similarly, type 4 lead-acid cells deliver about 69%, 90%, 110%, and 120% capacity at -20 , 0, 25 and 50 °C, respectively, in relation

to the respective values of 58%, 79%, 100%, and 107% obtained for type 3 lead-acid cells.

In order to obtain the self-discharge data for type 1 and type 2 lead-acid cells, the cells were left standing for 45 days and subsequently discharged at C/5 rate at 25 °C (Figure 12). The data show a capacity loss of only about 4% for type 2 lead-acid cells (Figure 12(b)). Under identical conditions, type 1 lead-acid cells exhibited a capacity loss as high as about 24% (Figure 12 (a)). Similarly, self-discharge data for type 3 and type 4 lead-acid cells were obtained after their storage for 30 days at 25 °C. The cells were subsequently discharged at C/5 rate (Figure 13). The data show a capacity loss of about 7% for type 4 cells (Figure 13(b)). Under identical conditions, type 3 lead-acid cells exhibited a capacity loss as high as about 13% (Figure 13(a)). A higher self-discharge value for negative-limited configuration could be envisaged in the light of the high oxygen reduction at the negative plate.

Cycle-life data obtained at C/5 rate for type 1 and type 2 lead-acid cells at 25 °C are shown in Figure 14. The data show a capacity fade of 10% and 4% for type 1 and type 2 lead-acid cells over 100 cycles. Similarly, cycle-life data obtained at C/5 rate for type 3 and type 4 lead-acid cells at 25 °C reflect a capacity fade of 14% and 7% for type 3 and type 4 lead-acid cells, respectively, over 100 cycles (Figure 15).

To study the structural changes occurring during the charge–discharge of conventional and PANI-coated negative plates, powder XRD patterns of the plates were taken as shown in Figure 16. The XRD patterns for a conventional negative plate in its fully discharged

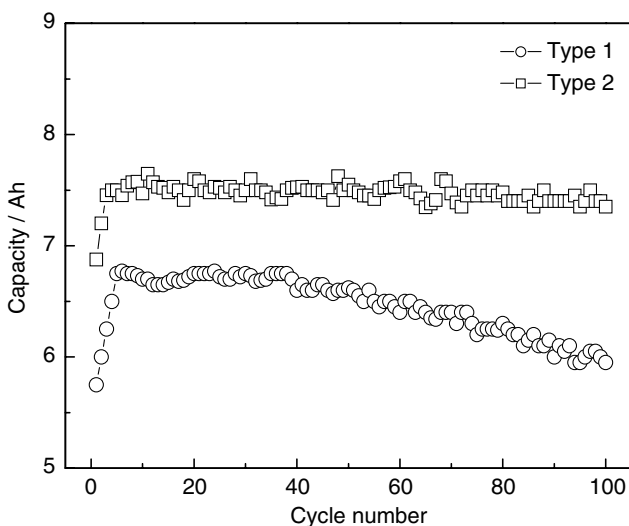


Fig. 14. Cycle-life data for type 1 and type 2 lead-acid cells at 25 °C.

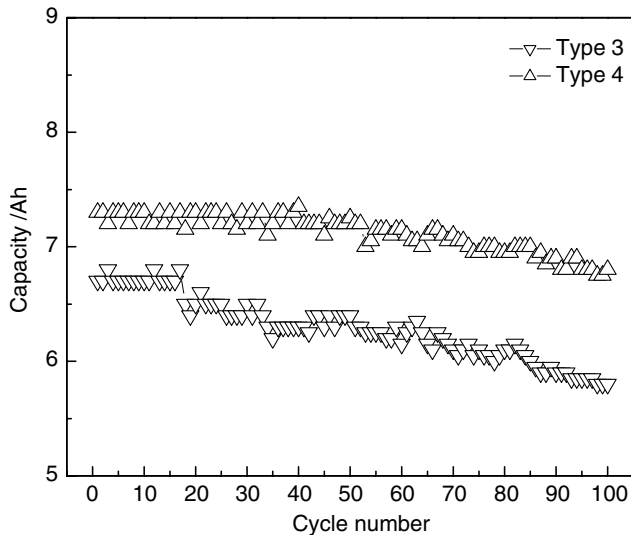


Fig. 15. Cycle-life data for type 3 and type 4 lead-acid cells at 25 °C.

(SoC = 0) and fully charged-state (SoC = 1) are shown in Figure 16(a) and (b), respectively; corresponding XRD patterns for a PANI-coated negative plate are shown in Figure 16(c) and (d), respectively. XRD patterns of fully charged conventional and PANI-coated negative plates, shown in Figure 16(b) and (d), respectively, clearly indicate that the conversion of lead from lead sulfate is more facile in the latter.

To examine the chemical nature of PANI film deposited onto the cured conventional negative plates, a part of PANI film was scraped out from the plate, and its IR spectrum was recorded as shown in Figure 17. The spectrum shows: (a) the absorbance peak at 1592 cm^{-1} corresponding to $\text{N}=\text{Q}=\text{N}$ stretching, (b) the absorbance peak at 1511 cm^{-1} corresponding to $\text{N}-\text{B}-\text{N}$ stretching, (c) the absorbance peak at 1375 cm^{-1} corresponding to $\text{C}-\text{N}$ stretching in QB_iQ , (d) the absorbance peak at 1250 cm^{-1} corresponding to $\text{C}-\text{N}$

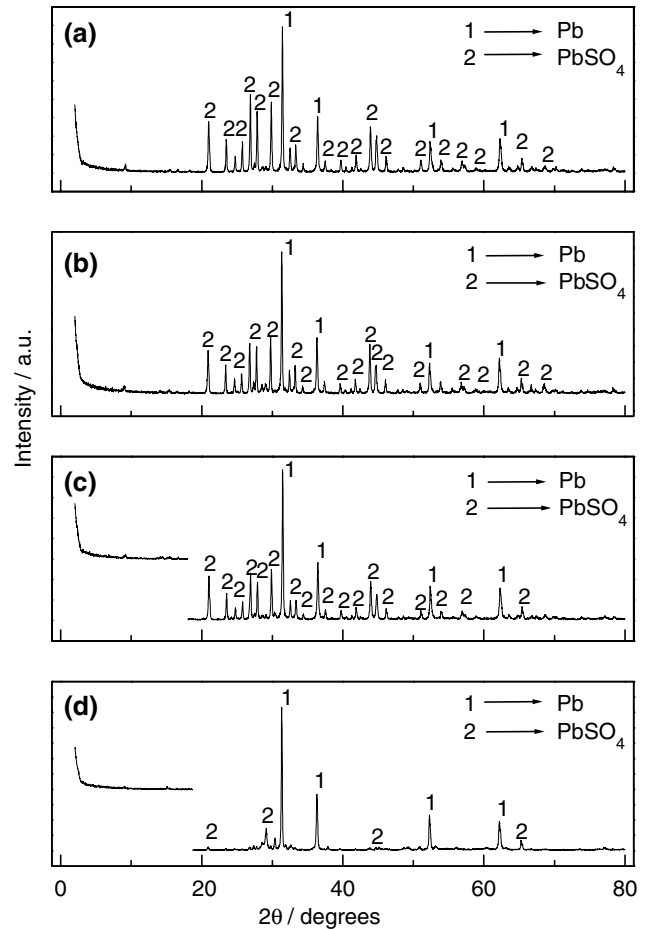


Fig. 16. Powder XRD pattern of (a) fully discharged conventional negative plate, (b) fully charged conventional negative plate, (c) fully discharged PANI-coated negative plate and (d) fully charged PANI-coated negative plate. In all the XRD patterns only prominent peaks have been labeled.

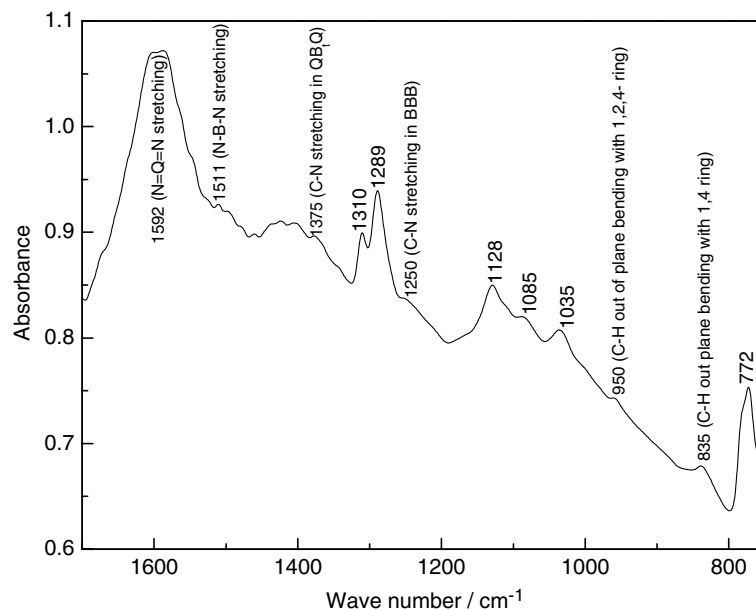


Fig. 17. IR-spectrum of PANI-film deposited on a cured conventional negative plate from 1 v/o of PANI in 0.15 M oxalic acid.

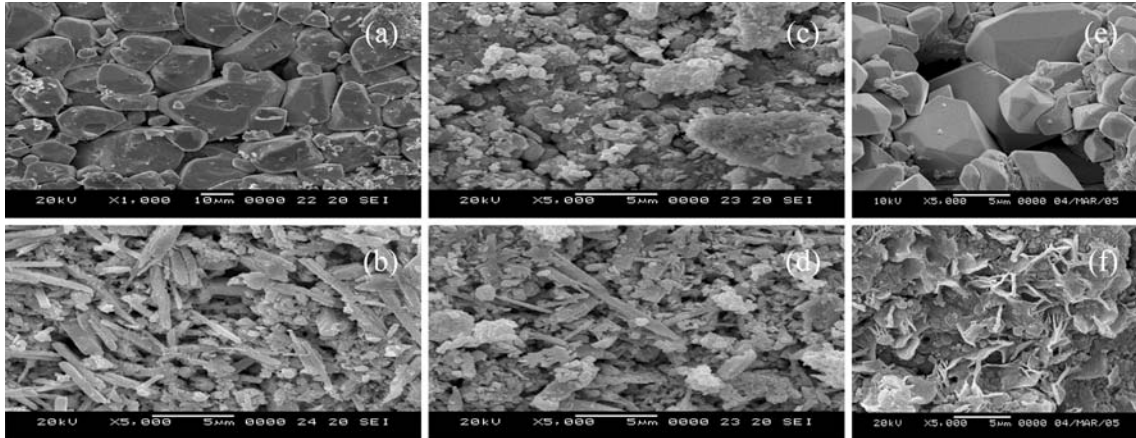


Fig. 18. Electrode surface morphologies of the conventional negative plate and PANI-coated negative plate in cured states: (a) and (b), formed states: (c) and (d), fully discharged state: (e) and (f), respectively.

stretching in BBB, (e) the absorbance peak at 1128 cm^{-1} corresponding to C–H in plane of bending with 1,2,4-ring, (f) the absorbance peak at 950 cm^{-1} corresponding to C–H out-of-plane bending with 1,2,4-ring, (g) the absorbance peak at 835 cm^{-1} corresponding to C–H out-of-plane bending with 1,4-ring. In the aforesaid description, Q stands for C_6H_4 -ring in quinoid form, B for C_6H_4 ring in benzenoid form, and B_t represents *trans*-orientation of C_6H_4 ring in benzenoid form.

Electrode surface morphologies of negative plates with and without PANI coating as seen under the scanning electron microscope are presented in Figure 18. The microstructure of cured conventional negative plates shown in Figure 18(a) depicts Pb and PbSO_4 crystals of undefined morphology. By contrast, the micrograph for the cured PANI-coated negative plate, shown in Figure 18(b), shows PANI particles of about $3.5\text{ }\mu\text{m}$ in the active material. The micrographs of

formed conventional and PANI-coated negative plates shown in Figure 18(c) and (d), respectively, suggest the active material to be interlocked with PANI-particles in the PANI-coated negative plate. The micrographs for the conventional and PANI-coated negative active mass in their fully discharged state are shown in Figure 18(e) and (f), respectively. It is evident that the active material remains interlocked in the PANI-coated negative plate even after it is fully discharged. It is also noteworthy that the PANI-coated negative plates do not undergo structural and morphological changes even after prolonged dipping in PANI containing oxalic acid solution as shown from the SEM pictures in Figure 19.

Impedance spectra for type 1, type 2, type 3 and type 4 lead-acid cells were obtained at various SoC values between 1 and 0. Typical impedance spectra for type 1 and type 2 cells at $\text{SoC} \sim 0.6$ are shown as Nyquist plots in Figure 20. Similarly, impedance spectra for type 3



Fig. 19. Electrode surface morphologies of the cured conventional negative plate after treatment with PANI dissolved in oxalic acid solution.

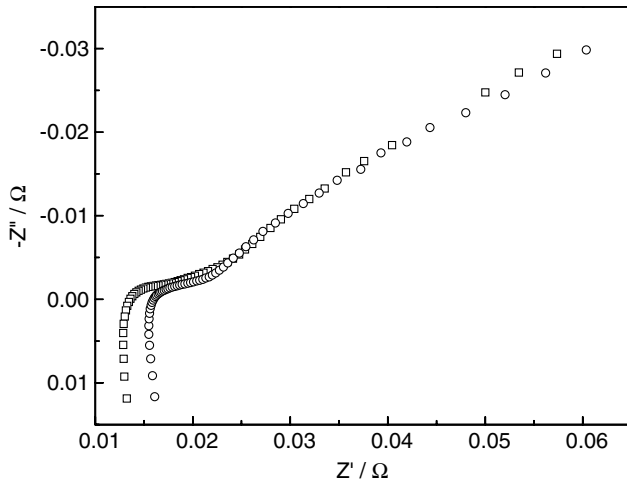


Fig. 20. Impedance spectrum for (○) type 1 and (□) type 2 lead-acid cells at SoC ~ 0.6 represented in Nyquist plot of imaginary part (Z'') vs. real part (Z').

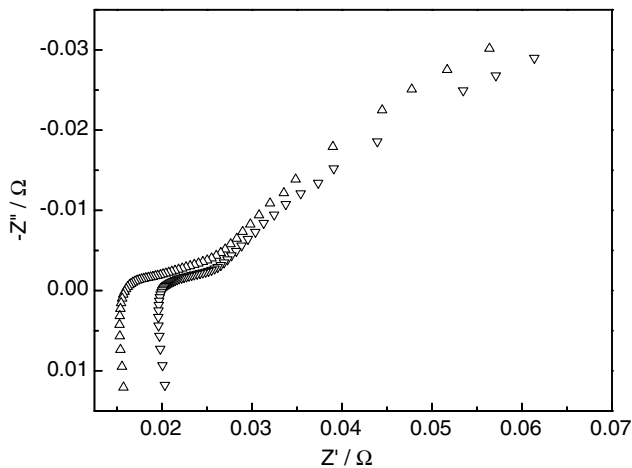


Fig. 21. Impedance spectrum for (▽) type 3 and (△) type 4 lead-acid cells at SoC ~ 0.5 represented in Nyquist plot of imaginary part (Z'') vs. real part (Z').

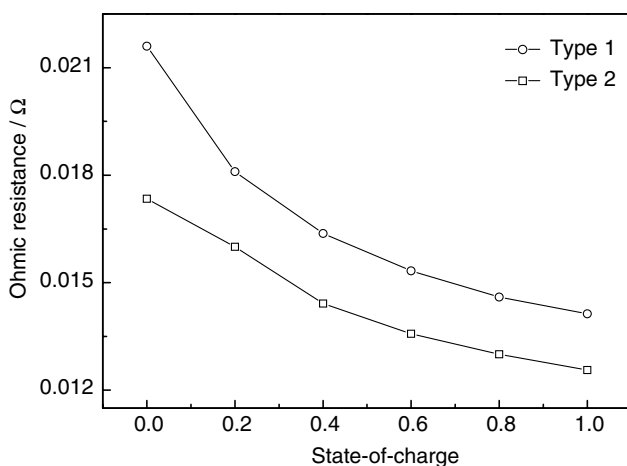


Fig. 22. The variation in ohmic resistance with state-of-charge for (○) type 1 and (□) type 2 lead-acid cells.

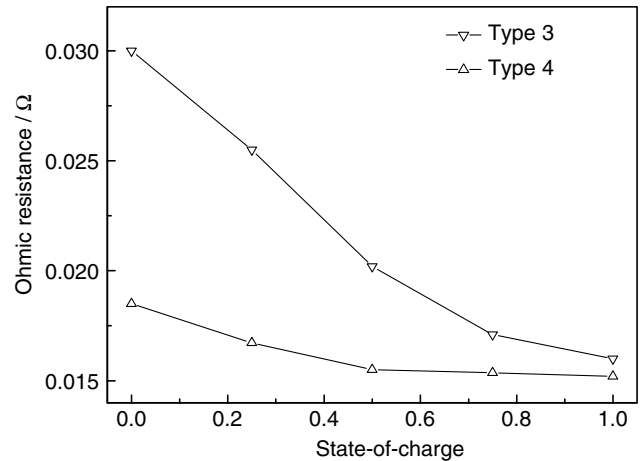


Fig. 23. The variation in ohmic resistance with state-of-charge for (▽) type 3 and (△) type 4 lead-acid cells.

and type 4 lead-acid cells at SoC ~ 0.5 are shown as Nyquist plots in Figure 21. The Nyquist plots in Figures 20 and 21 comprise an inductive distribution of the data at frequencies > 0.004 kHz followed by two capacitive semicircles in the frequency range between 0.004 kHz and 10 mHz. The ohmic resistance data for type 1 and type 2 lead-acid cells are shown in Figure 22. Similarly, the ohmic resistance data for type 3 and type 4 lead-acid cells are shown in Figure 23. The data suggest that the ohmic resistance of type 2, and type 4 lead-acid cells are lower in relation to their values for type 1 and type 3 lead-acid cells at all SoC values between 1 and 0. From the foregoing, it is conjectured that both type 2 and type 4 lead-acid cells can sustain high discharge-rates in relation to type 1 and type 3 lead-acid cells with prolonged cycling capability, a desired feature for hybrid electric-vehicle batteries that operate on partial-state-of-charge.

4. Conclusions

It is demonstrated that lead-acid cells with polyaniline-coated negative plates can sustain higher discharge-rates for prolonged cycles with little loss in their capacity. This study would help designing lead-acid batteries suitable for operation at partial-state-of-charge.

References

1. R.H. Newnham and W.G.A. Balasing, *J. Power Sources* **107** (2002) 273.
2. P.T. Moseley, *J. Power Sources* **127** (2004) 27.
3. L.T. Lam, R.H. Newnham, H. Ozgun and F.A. Fleming, *J. Power Sources* **88** (2000) 92.
4. P.T. Moseley and A.D. Turner, *J. Power Sources* **9** (1982) 19.
5. B. Culpin and D.A.J. Rand, *J. Power Sources* **39** (1991) 415.
6. M. Shiomi, T. Funato, K. Nakamura, K. Takahashi and M. Tsubota, *J. Power Sources* **67** (1997) 147.
7. D. Berndt, *Maintenance-Free Batteries*, 2nd ed., (Wiley, New York, 1997).

8. A. Cooper and P.T. Moseley, *J. Power Sources* **113** (2003) 200.
9. P. Ruetschi, *J. Power Sources* **127** (2004) 33.
10. D. Pavlov, B. Monakhov, M. Maja and N. Penazzi, *J. Electrochem. Soc.* **136** (1989) 27.
11. D. Pavlov, A. Dakhouche and T. Rogachev, *J. Power Sources* **30** (1990) 117.
12. M. Tsubota, S. Osumi and M. Kosai, *J. Power Sources* **33** (1991) 105.
13. D. Pavlov, *J. Power Sources* **33** (1991) 221.
14. A.F. Hollenkamp, *J. Power Sources* **36** (1991) 567.
15. T. Laitinen, K. Salmi, G. Sundholm, B. Monahov and D. Pavlov, *Electrochim. Acta* **36** (1991) 605.
16. D. Pavlov, B. Monahov, G. Sundholm and T. Laitinen, *J. Electroanal. Chem.* **305** (1991) 57.
17. A.F. Hollenkamp, K.K. Constanti, A.M. Huey, M.J. Koop and L. Apuleanu, *J. Power Sources* **40** (1992) 125.
18. G.J. May, *J. Power Sources* **53** (1995) 111.
19. R. Wagner, *J. Power Sources* **53** (1995) 153.
20. L.T. Lam, H. Ozgun, O.V. Lim, J.A. Hamilton, L.H. Vu, D.G. Vella and D.A.J. Rand, *J. Power Sources* **53** (1995) 215.
21. K.K. Constanti, A.F. Hollenkamp, M.J. Koop and K. McGregor, *J. Power Sources* **55** (1995) 269.
22. K. Peters, *J. Power Sources* **59** (1996) 6.
23. P.T. Moseley, *J. Power Sources* **59** (1996) 81.
24. A.F. Hollenkamp, *J. Power Sources* **59** (1996) 87.
25. K. Nakamura, M. Shiomi, K. Takahashi and M. Tsubota, *J. Power Sources* **59** (1996) 153.
26. M. Shiomi, Y. Okada, Y. Tsuboi, S. Osumi and M. Tsubota, *J. Power Sources* **113** (2003) 271.
27. D.A.J. Rand, D.P. Boden, C.S. Lakshmi, R.F. Nelson and R.D. Prengman, *J. Power Sources* **107** (2002) 280.
28. D.A.J. Rand, R. Woods and R.M. Dell, *Batteries for Electric Vehicles* (Research Studies Press Ltd., 1998).
29. D.C. Trivedi, in H.S. Nalwa (Ed.), *Handbook of Organic Conductive Molecules and Polymers*, Vol. 2 (Wiley, New York, 1997) p. 504.
30. B.A. Boukamp, *Equivalent Circuit User Manual* (University of Twente, The Netherlands, 1988/89).